

Revisiting Maximum Entropy Inverse Reinforcement Learning: New Perspectives and Algorithms

Aaron J. Snoswell* Surya P. N. Singh[†] Nan Ye[‡]

December 22, 2024

Abstract

We provide new perspectives and inference algorithms for Maximum Entropy (MaxEnt) Inverse Reinforcement Learning (IRL), which provides a principled method to find a most non-committal reward function consistent with given expert demonstrations, among many consistent reward functions.

We first present a generalized MaxEnt formulation based on minimizing a KL-divergence instead of maximizing an entropy. This improves the previous heuristic derivation of the MaxEnt IRL model (for stochastic MDPs), allows a unified view of MaxEnt IRL and Relative Entropy IRL, and leads to a model-free learning algorithm for the MaxEnt IRL model. Second, a careful review of existing inference algorithms and implementations showed that they approximately compute the marginals required for learning the model. We provide examples to illustrate this, and present an efficient and exact inference algorithm. Our algorithm can handle variable length demonstrations; in addition, while a basic version takes time quadratic in the maximum demonstration length L , an improved version of this algorithm reduces this to linear using a padding trick.

*School of Information Technology and Electrical Engineering, The University of Queensland

[†]Intuitive Surgical

[‡]School of Mathematics and Physics, The University of Queensland

Experiments show that our exact algorithm improves reward learning as compared to the approximate ones. Furthermore, our algorithm scales up to a large, real-world dataset involving driver behaviour forecasting. We provide an optimized implementation compatible with the OpenAI Gym interface. Our new insight and algorithms could possibly lead to further interest and exploration of the original MaxEnt IRL model.

1 Introduction

Inverse Reinforcement Learning (IRL) searches for a reward or cost function to rationalize observed behaviour. This is challenging because the same reward may be optimized by different behaviors, and optimizing different reward functions can lead to the same behavior. In their seminal work Ziebart *et al.* developed a principled solution using the Maximum Entropy (MaxEnt) principle to choose the most non-committal consistent reward [19] – *i.e.* a reward which matches demonstrated feature counts but makes no additional assumptions about the demonstrated behaviour. Variations of this idea have seen great success in many recent works — including models based on causal entropy [18, 17], and efficient sample-based methods that maximize state-conditioned policy entropy [8, 9].

Despite the long line of works based on the original MaxEnt IRL paper, we believe that the full value of the original MaxEnt IRL model might not have been fully realized yet, for two reasons. First, while the MaxEnt IRL model for deterministic Markov Decision Processes (MDPs) has been rigorously derived from the MaxEnt principle, the corresponding model for stochastic MDPs was based on a heuristic argument. While this has motivated alternative formulations such as causal Maximum Causal Entropy (MaxCausalEnt) IRL [18], we were also interested to know whether there is a simple and rigorous justification of the MaxEnt IRL model for stochastic MDPs, which might bring new insight. Second, the published inference (*i.e.*, marginal computation) algorithms [19, 20] for MaxEnt IRL only approximately compute the marginals required for learning – as confirmed by the original authors.¹ Existing implementations online have largely followed these algorithms and are approximate. While approximate algorithms are often sufficient for achieving good generalization performance, we are inter-

¹Personal correspondence with B. Ziebart.

ested in developing exact algorithms in this case, and study whether they can achieve better reward learning than approximate algorithms.

Motivated by the above questions, we revisit the MaxEnt IRL model and present some new perspectives, algorithms, and empirical insights.

1. We provide a simple and rigorous derivation of the original MaxEnt IRL model using the Kullback-Liebler divergence, without using any heuristic argument. Our derivation provides a unified view for MaxEnt IRL and relative entropy IRL [3], and highlights a key difference between these two frameworks. In addition, the connection between them suggests an model-free importance sampling algorithm for learning a MaxEnt IRL model (Section 4).
2. We present an efficient exact forward-backward inference algorithm. This allows exact computation of the gradients used in reward learning. Unlike previous work, our algorithm does not assume that the demonstrations are of the same length. While this increases the time complexity from linear in L to quadratic in L , we bring the time complexity back to linear in L using a padding trick (Section 5).
3. We illustrate that published MaxEnt IRL algorithms [19, 20] are approximate, and empirically show that exact algorithms improve reward learning. In addition, we show that our algorithm can scale up to a large, real-world dataset involving driver behaviour forecasting (Section 6).
4. We provide an open-source optimized reference implementation of our algorithms, compatible with the OpenAI Gym MDP interface to allow easy application to many problems.

Finally, we conclude with a discussion on opportunities for future work (Section 7).

2 Related Work

MaxEnt IRL theory was proposed in [19, 17]. This framework has seen great success, and many extensions of this model have been proposed e.g. for continuous state and action spaces [2, 10] or using deep non-linear reward representations [16, 7]. As pointed out in the introduction, we present a

simple derivation of MaxEnt IRL that improves the original heuristic derivation, leading to a unified view of the original theoretical framework [19] and the Relative Entropy (RE) IRL method [3]. In addition, the unified view directly leads to a model-free learning algorithm for MaxEnt IRL, which is an analogue of that for RE-IRL.

The basic version of our algorithm is adapted from the exact inference algorithms for linear-chain conditional random fields [12]. We present our algorithm in a form that supports any combination of state-, state-action, and/or state-action-state features. In addition, our algorithm has several important features that make it flexible: (a) It does not require the demonstration trajectories to be of the same length, and is thus capable of handling variable length demonstrations, and (b) Our algorithm also supports discounting, episodic or continuing MDPs, and MDPs with state-dependent action sets, and a straight-forward application of the methods from [16] can extend our algorithm to the case of learned non-linear reward functions, such as a deep neural networks. Importantly, while adding support for variable-length paths increases the time complexity of our basic algorithm, we are able to achieve linear time complexity in the length of the longest demonstration path L using a padding trick.

Our algorithms can be viewed as special cases of the well-known sum-product algorithm for graphical models [11]. This perspective allows extending our algorithm to handle more complex features. We leave this to future work.

3 Inverse Reinforcement Learning

As in most works, we consider IRL for an MDP $\mathcal{M} = \{\mathcal{S}, \mathcal{A}, p_0, T, R, \gamma\}$, with discrete states $s \in \mathcal{S}$, discrete actions $a \in \mathcal{A}$, starting state distribution $p_0(s)$, transition dynamics $T = p(s' | s, a)$, reward function $R(s)$, and discount factor $\gamma \in [0, 1]$. A policy $\pi(a | s)$ provides a (stochastic) mapping from states to actions and describes a strategy to navigate the MDP. A sample from a policy is a state-action trajectory $\tau = ((s_1, a_1), \dots, (s_T, \text{None}))$ with length denoted by $|\tau|$.

In our IRL setting, we are provided with a set of demonstration trajectories $\mathcal{D} = \{\tau_1, \dots, \tau_N\}$, and a partial MDP definition $\mathcal{M} \setminus R$ – *i.e.* we know the MDP dynamics, but not the reward function. The goal is to identify a reward function R such that the demonstration data appear ‘optimal’ according to

some criteria (e.g. maximizing cumulative γ -discounted rewards).

Abbeel and Ng [1] showed that for an MDP with its reward $R(s)$ linear in the feature vector $\phi(s)$, to learn a policy π with the same value as the demonstrator, it suffices to match *feature expectations*, i.e., choose a reward that induces a policy π such that

$$\mathbb{E}_{\tau \sim \pi}[\phi(\tau)] = \mathbb{E}_{\tau \sim \mathcal{D}}[\phi(\tau)],$$

where $\mathbb{E}_{\tau \sim \mathcal{D}}[\phi(\tau)] = \frac{1}{|\mathcal{D}|} \sum_{\tau \in \mathcal{D}} \phi(\tau)$, where for a trajectory $\tau = ((s_1, a_1), \dots, (s_{|\tau|}, \text{None}))$, the vector $\phi(\tau) = \sum_{t=1}^{|\tau|} \gamma^{t-1} \phi(s_t)$ is the discounted feature vector accumulated along τ . While a useful starting point, this problem is ill-posed, because generally, many policies have matching feature expectations. The problem is further complicated by the fact that positive-linear or potential-based ‘shaping’ transformations of the true reward all have the same optimal policies [14].

Early IRL methods generally relied on heuristics or probabilistic assumptions to resolve the ambiguity of a consistent reward. The MaxEnt IRL approach provides a principled way to do this.

4 The Principle of Maximum Entropy

The MaxEnt IRL model defines a distribution on the set \mathcal{T} of all feasible trajectories as

$$p_{\theta}(\tau) \triangleq \frac{q(\tau)e^{\theta^\top \phi(\tau)}}{Z_{\theta}}, \quad (1)$$

where q is the (un-normalized) distribution induced by MDP dynamics alone

$$q(\tau) \triangleq p_0(s_1) \prod_{t=1}^{|\tau|-1} T(s_{t+1} | s_t, a_t),$$

and $Z_{\theta} \triangleq \sum_{\tau' \in \mathcal{T}} q(\tau')e^{\theta^\top \phi(\tau')}$ is the normalizing constant often known as the *partition function*. In addition, the parameters θ are chosen to maximize the log-likelihood given \mathcal{D}^2

$$\ell(\theta) = \theta^\top \mathbb{E}_{\tau \sim \mathcal{D}}[\phi(\tau)] + \frac{1}{|\mathcal{D}|} \sum_{\tau \in \mathcal{D}} \log q(\tau) - \log Z_{\theta}, \quad (2)$$

²*N.b.* A previously published version of this paper was missing the log operator before q in Eq. 2 - the updated expression here is correct.

We can interpret $p_{\theta}(\tau)$ as a non-stationary policy, and the exponentiated term in Eq. 1 as a reward function linear in the transition features *viz.*,

$$\begin{aligned} R(\tau) &\triangleq \boldsymbol{\theta}^\top \boldsymbol{\phi}(\tau) = \boldsymbol{\theta}^\top \sum_{t=1}^{|\tau|} \gamma^{t-1} \boldsymbol{\phi}(s_t) = \sum_{t=1}^{|\tau|} \gamma^{t-1} \boldsymbol{\theta}^\top \boldsymbol{\phi}(s_t) \\ &= \sum_{t=1}^{|\tau|} \gamma^{t-1} R(s_t). \end{aligned}$$

Non-stationary policies are more expressive than stationary policies, and the MaxEnt IRL framework allows all possible behaviors to be jointly learned due to global normalization. This makes it potentially more powerful in complex domains, as compared to models which learn a stationary policy or do not perform global normalization.

As a contribution of this paper, we show that the MaxEnt IRL model is the solution of

$$\begin{aligned} \min_p \quad & D_{\text{KL}}(p \parallel q) & (3) \\ \text{s.t.} \quad & \mathbb{E}_{\tau \sim p}[\boldsymbol{\phi}(\tau)] = \mathbb{E}_{\tau \sim \mathcal{D}}[\boldsymbol{\phi}(\tau)], \\ & \sum_{\tau \in \mathcal{T}} p(\tau) = 1, \\ & p(\tau) \geq 0 \quad \forall \tau \in \mathcal{T}. \end{aligned}$$

The feature moment matching constraint ensures the learned non-stationary policy p will match the preferences demonstrated in the data, while the minimization objective forces the model close to the natural dynamics of the MDP. These lead to a unique reward solution, thus resolving the reward ambiguity problem. Our derivation is simple and similar to that for RE-IRL [3], and we defer it to Appendix 8.

We highlight here a few new insights from this interpretation. First, this interpretation shows that the MaxEnt IRL model chooses a model that best agrees with the transition dynamics under the feature matching constraints. Second, RE-IRL and MaxEnt IRL are the same, however they use different reference distributions q . Specifically, the reference distribution used in RE-IRL is $q_{\pi_0}(\tau) = q(\tau)w_{\pi_0}(\tau)$, where π_0 is a baseline policy, and $w_{\pi_0} = \prod_{t=1}^{|\tau|-1} \pi_0(a_t \mid s_t)$. While MaxEnt IRL and RE-IRL can now be seen as special cases of a unified model, this also reveals a subtle but important

difference: RE-IRL aims to agree with a baseline policy and the transition dynamics, while MaxEnt IRL aims to agree with the transition dynamics only. If we only consider trajectories of the same length, then MaxEnt IRL can be seen as RE-IRL with a uniform baseline policy. Third, such a connection between MaxEnt IRL and RE-IRL allows us to directly adapt the model-free importance sampling learning algorithm for RE-IRL to MaxEnt IRL: we simply replace all occurrences of $w_{\pi_0}(\tau)$ with the value ‘1’ in their gradient estimator (*cf.* Eq. (8) in [3]). However, this approach may be biased towards shorter demonstrations as they will have larger weights in the estimator. We omit the details here and focus on our exact algorithms below for brevity.

5 A New Algorithm

To learn the MaxEnt IRL model in Eq. 1, we need to maximize the log-likelihood, which is convex in θ and thus can be maximized using standard gradient-based methods — in our experiments we used L-BFGS-B. The value and the gradient of the log-likelihood, required in the optimization algorithm, can be computed using the partition function Z_θ and the marginal state distribution $p_{\theta,t}(s)$, which denotes the probability that the t -th state is s for τ sampled from the MaxEnt distribution $p_\theta(\tau)$. Specifically, with the partition function, we can easily compute the log-likelihood using Eq. 1; with the marginals, we can compute the gradient as follows

$$\nabla \ell(\theta) = \mathbb{E}_{\tau \sim \mathcal{D}}[\phi(\tau)] - \sum_{s \in \mathcal{S}} \phi(s) \sum_{t=1}^L p_{\theta,t}(s). \quad (4)$$

Explicit computation of the partition function Z_θ grows exponentially in time for longer demonstration paths, however the (first order) Markov property of the MDP allows us to decompose the partition and marginal feature values recursively with an efficient forward-backward algorithm.

This was previously attempted in [19], and in an updated version of that paper [20], however their algorithm relied on a heuristic for the case of stochastic MDPs. We find that this leads to approximate gradients (see proofs in Appendix 9) and negatively impacts the reward learning process (see experiments in Section 6). We also note that these algorithms were derived only for the case of un-discounted MDPs with state-based rewards —

our algorithm adds support for discounted MDPs, and for MDPs with reward functions consisting of any combination of state-, state-action, and/or state-action-state features (our derivations focus on the case of state-based rewards for brevity, however in Fig. 1 we provide the full algorithm with support for general reward structure).

Complementing and extending these previous works, we construct a novel dynamic program that computes MaxEnt IRL gradients that are exact, even for the case of stochastic MDPs. The algorithm utilizes partial versions of the partition function, known as message-passing variables,³ which we describe below.

5.1 Forward message passing variable

We assume all trajectories in \mathcal{T} have length at most L . We define a forward message-passing variable that computes the partition contribution for paths of length l that *end* at a given state s ,

$$\alpha_l(s) \triangleq \sum_{\tau \in \mathcal{T}: |\tau|=l, \tau_l=s} q(\tau) e^{R(\tau)} \quad 1 \leq l \leq L.$$

Un-rolling this definition leads to a recurrence for $\alpha_l(s)$,

$$\begin{aligned} \alpha_1(s) &= p_0(s) e^{R(s)} \\ \alpha_{l+1}(s') &= \sum_{(s,a) \in \mathcal{P}(s')} \alpha_l(s) T(s' | s, a) e^{\gamma^l R(s')} \quad 1 \leq l < L, \end{aligned}$$

where $\mathcal{P}(s)$ denotes the parent set of state-action tuples that can immediately precede s according to the MDP dynamics.

5.2 Backward message passing variable

We define an analogous backward message-passing variable which counts the partition contribution for length t suffixes within paths of total length l , where the path suffix *starts* at a given state s ,

$$\begin{aligned} \beta_{l,t}(s) &\triangleq \sum_{\tau \in \mathcal{T}: |\tau|=l, \tau_1=(s,\cdot)} q'(\tau) e^{R(\tau)} \quad 1 \leq l \leq L, \\ &\quad 1 \leq t \leq l, \end{aligned}$$

³The name comes from Dynamic Programming literature and is due to the passing of probability ‘messages’ forward and backward through the MDP dynamics.

where $q'(\tau)$ is the same as $q(\tau)$, but does not include the starting state distribution. Un-rolling the definition of $\beta_{l,t}(s)$ gives an analogous recurrence;

$$\begin{aligned}\beta_{l,1}(s) &= e^{\gamma^{l-1}R(s)} \\ \beta_{l,t+1}(s) &= \sum_{(a,s') \in \mathcal{C}(s)} T(s' | s, a) e^{\gamma^{l-t-1}R(s)} \beta_{l,t}(s')\end{aligned}\quad 1 \leq l \leq L, 1 \leq t < l,$$

where $\mathcal{C}(s)$ denotes the child set of action-state tuples that can immediately succeed s according to the MDP dynamics.

5.3 Partition and marginal calculations

Now we describe the dynamic program to compute the terms of interest. For a set of paths of lengths $1 \leq l \leq L$ the partition function value is given by

$$Z_{\theta} = \sum_{l=1}^L \sum_{s \in \mathcal{S}} \alpha_l(s),$$

and the marginal state distributions at times $1 \leq t \leq L$ are given by

$$p_{\theta,t}(s) = \frac{1}{Z_{\theta}} \alpha_t(s) \left(1 + \sum_{(a,s') \in \mathcal{C}(s)} T(s' | s, a) \sum_{l=t+1}^L \beta_{l,l-t}(s') \right).$$

This dynamic program will compute the partition and marginal state values exactly, however requires storing $\beta_{l,t}$ for $1 \leq t \leq l \leq L$, and has polynomial time complexity $\mathcal{O}(|\mathcal{S}|^2 |\mathcal{A}| L^2)$, where L is the length of the longest path in the demonstration dataset. We show in the following section how a padding trick can be used to compute the same results linearly in L , and with less space required for the backward message variable β .

5.4 A padding trick improves computational complexity

By augmenting the MDP dynamics with an auxiliary state and action we can achieve a more efficient algorithm that still computes exact gradients. For all sequences shorter than the longest demonstration path length $L = \max_{\tau \in \mathcal{D}} |\tau|$, we pad them with auxiliary actions and states $((\cdot, a_a), (s_a, \cdot))$

until the sequence length is L . For example, a $|\tau| = 2$ sequence would be padded to length $L = 4$ as follows;

$$\begin{aligned} & ((s_1, a_1), (s_2, \mathbf{None})) \\ \implies & ((s_1, a_1), (s_2, a_a), (s_a, a_a), (s_a, \mathbf{None})). \end{aligned}$$

To ensure exact gradients are computed, the modified MDP must satisfy the following rules:

1. Auxiliary states have zero starting probability,

$$p_0(s_a) \triangleq 0$$

2. Auxiliary states are absorbing, and are reachable from any state when the auxiliary action is chosen,

$$T(s_a | s_t, a_t) \triangleq \begin{cases} 1 & s_t = s_a, \forall a_t \in \mathcal{A} \\ 1 & s_t \neq s_a, a_t = a_a \\ 0 & \text{otherwise} \end{cases}$$

$$\text{s.t. } \mathcal{C}(s_a) \triangleq \{(a_a, s_a)\},$$

$$\mathcal{P}(s_a) \triangleq \{(s, a_a) : \forall s \in \mathcal{S}\},$$

$$\mathcal{C}(s) \supseteq \{(a_a, s_a)\} \quad \forall s \in \mathcal{S}.$$

3. The auxiliary state and action should not modify the rewards encountered along any path,

$$R(s_a) \triangleq 0$$

5.5 Padded message passing variables

The backward message passing variable $\alpha_l(s)$ is computed as before, for all paths of length $1 \leq l < L$. However due to the padded sequences, the forward message passing variable $\beta_{l,t}(s)$ only needs to be computed and stored for $l = L$,

$$\begin{aligned} \beta_{L,1}(s) &= e^{\gamma^{L-1}R(s)} \\ \beta_{L,t+1}(s) &= \sum_{(a,s') \in \mathcal{C}(s)} T(s' | s, a) e^{\gamma^{L-t-1}R(s)} \beta_{L,t}(s') \quad 1 \leq t < L. \end{aligned}$$

5.6 Padded partition and marginal calculations

With the padded MDP formulation, the partition function is then given by

$$Z_{\theta} = \sum_{l=1}^L \sum_{s \in \mathcal{S} \setminus \{s_a\}} \alpha_l(s),$$

and the update for state marginal distributions no longer needs a summand over variable suffix lengths, thus reducing the time complexity. That is,

$$p_{\theta,t}(s) = \begin{cases} \frac{1}{Z_{\theta}} \alpha_t(s) & t = L \\ \frac{1}{Z_{\theta}} \alpha_t(s) \sum_{(a,s') \in \mathcal{C}(s)} T(s' | s, a) \beta_{L,L-t}(s') & \text{otherwise,} \end{cases}$$

which is computed for $1 \leq t \leq L$ and states $s \in \mathcal{S} \setminus \{s_a\}$.

This algorithm computes the same (exact) gradients as the basic algorithm described above in Section 5.3, however has linear time complexity in the size of the longest demonstration path $\mathcal{O}(|\mathcal{S}|^2 |\mathcal{A}| L)$.

5.7 Pseudo-code listing

For brevity, the derivations in the previous sections show the case of a reward based only on state features. With careful consideration to the bounds of various summands, the above results generalize in a straight-forward manner to the case of rewards that include any combination of state-, state-action, and/or state-action-state features. That is,

$$\begin{aligned} R(\tau) &\triangleq \sum_{t=1}^{|\tau|} \gamma^{t-1} \theta_s^{\top} \phi_s(s_t) \\ &\quad + \sum_{t=1}^{|\tau|-1} \gamma^{t-1} (\theta_{sa}^{\top} \phi_{sa}(s_t, a_t) + \theta_{sas'}^{\top} \phi_{sas'}(s_t, a_t, s_{t+1})) \\ &= \sum_{t=1}^{|\tau|} \gamma^{t-1} R_s(s_t) \\ &\quad + \sum_{t=1}^{|\tau|-1} \gamma^{t-1} (R_{sa}(s_t, a_t) + R_{sas'}(s_t, a_t, s_{t+1})). \end{aligned}$$

The necessary modifications to the padding trick are that we define $R(s, a_a) = R(s, a_a, s_a) = 0, \forall s \in \mathcal{S}$.

Input: $\mathcal{M} \setminus R, \mathcal{D}, \phi_s, \phi_{sa}, \phi_{sas'}$
Output: $\theta = \{\theta_s, \theta_{sa}, \theta_{sas'}\}, Z_\theta$

- 1 $L = \max_{\tau \in \mathcal{D}} |\tau|$
- 2 $\overline{\phi_s} = \frac{1}{|\mathcal{D}|} \sum_{\tau \in \mathcal{D}} \sum_{t=1}^{|\tau|} \gamma^{t-1} \phi_s(s_t)$
- 3 $\overline{\phi_{sa}} = \frac{1}{|\mathcal{D}|} \sum_{\tau \in \mathcal{D}} \sum_{t=1}^{|\tau|-1} \gamma^{t-1} \phi_{sa}(s_t, a_t)$
- 4 $\overline{\phi_{sas'}} = \frac{1}{|\mathcal{D}|} \sum_{\tau \in \mathcal{D}} \sum_{t=1}^{|\tau|-1} \gamma^{t-1} \phi_{sas'}(s_t, a_t, s_{t+1})$
- 5 $\theta_s = \theta_{sa} = \theta_{sas'} = \mathbf{0}$
- 6 **while not converged do**
- 7 $\alpha_1 = p_0(s) \exp(R(s))$
- 8 **for** $t \leftarrow 1 \dots L - 1$ **do**
- 9 $\alpha_{t+1} = \sum_{(s,a) \in \mathcal{P}(s')} \alpha_t(s) T(s' | s, a)$
 $\exp(\gamma^{t-1} R(s, a) + \gamma^{t-1} R(s, a, s') + \gamma^t R(s'))$
- 10 $\beta_{L,1} = \exp(\gamma^{L-1} R(s))$
- 11 **for** $t \leftarrow 1 \dots L - 1$ **do**
- 12 $\beta_{L,t+1} = \sum_{(a,s') \in \mathcal{C}(s)} T(s' | s, a)$
 $\exp(\gamma^{L-t-1} (R(s) + R(s, a) + R(s, a, s'))) \beta_{L,t}(s')$
- 13 $Z_\theta = \sum_{t=1}^L \sum_{s \in \mathcal{S} \setminus \{s_a\}} \alpha_t(s)$
- 14 **for** $t \leftarrow 1 \dots L - 1$ **do**
- 15 $p_{\theta,t}(s) = \frac{1}{Z_\theta} \alpha_t(s) \sum_{(a,s') \in \mathcal{C}(s)} T(s' | s, a)$
 $\exp(\gamma^{t-1} R(s, a) + \gamma^{t-1} R(s, a, s')) \beta_{L,L-t}(s')$
- 16 $p_{\theta,t}(s, a) = \frac{1}{Z_\theta} \alpha_t(s) \sum_{s' \in \mathcal{S}} T(s' | s, a)$
 $\exp(\gamma^{t-1} R(s, a) + \gamma^{t-1} R(s, a, s')) \beta_{L,L-t}(s')$
- 17 $p_{\theta,t}(s, a, s') = \frac{1}{Z_\theta} \alpha_t(s) T(s' | s, a)$
 $\exp(\gamma^{t-1} R(s, a) + \gamma^{t-1} R(s, a, s')) \beta_{L,L-t}(s')$
- 18 $p_{\theta,L}(s) = \frac{1}{Z_\theta} \alpha_L(s)$
- 19 $\nabla_{\theta_s} = \overline{\phi_s} - \sum_{s \in \mathcal{S}} \phi_s(s) \sum_{t=1}^L p_{\theta,t}(s)$
- 20 $\nabla_{\theta_{sa}} = \overline{\phi_{sa}} - \sum_{s \in \mathcal{S}, a \in \mathcal{A}} \phi_{sa}(s, a) \sum_{t=1}^{L-1} p_{\theta,t}(s, a)$
- 21 $\nabla_{\theta_{sas'}} = \overline{\phi_{sas'}} -$
 $\sum_{s \in \mathcal{S}, a \in \mathcal{A}, s' \in \mathcal{S}} \phi_{sas'}(s, a, s') \sum_{t=1}^{L-1} p_{\theta,t}(s, a, s')$
- 22 Update $\theta_s, \theta_{sa}, \theta_{sas'}$ using $\nabla_{\theta_s}, \nabla_{\theta_{sa}}, \nabla_{\theta_{sas'}}$ with
 chosen optimizer.
- 23 **return** $\theta = \{\theta_s, \theta_{sa}, \theta_{sas'}\}$ and Z_θ

Figure 1: ExactMaxEntIRL — Exact Maximum Entropy Inverse Reinforcement Learning

We list the complete uni-modal IRL algorithm pseudocode for this general reward structure in Fig. 1.

A naïve implementation of *any* MaxEnt algorithm may exhibit numerical floating-point overflow due to repeated exponentiation of rewards, especially for large positive reward values and/or long trajectories. This can be avoided by using (natural) log-space variables and the standard ‘log-sum-exp’ transform when implementing the algorithm.

Finally, note that with appropriate modifications to the children and parent set operators $\mathcal{C}(s)$ and $\mathcal{P}(s)$, our algorithm is also general enough to support MDPs with state-dependent action sets $\mathcal{A} = \bigcup_{s \in \mathcal{S}} \mathcal{A}(s)$.

We provide an optimized reference implementation of this algorithm as a stand-alone Python 3.6.9 package at our open-source code repository⁴. Our implementation is compatible with the OpenAI Gym MDP interface [4] to allow easy use with many problems, and we utilize the Numba Just-In-Time optimizing compiler [13] to achieve highly performant vectorized machine code for critical functions.

5.8 MaxEnt IRL Inference

After reward learning, the Maximum Likelihood (ML) path between two states or state-distributions $\tau_{\text{ML}} = \arg \max_{\tau \in \mathcal{T}} p_{\theta}(\tau)$ can be found using a straight-forward Viterbi type dynamic program that has polynomial time complexity — we omit this algorithm for brevity, but refer the reader to our project repository. Alternatively, if the learned weights are such that all transitions incur negative reward, any weighted shortest path search algorithm can be used (e.g. Dijkstra’s or Bellman-Ford), reducing the ML path inference time complexity.

6 Experimental Results

We verify the function of our algorithm using several synthetic MDPs from the OpenAI Gym library [4], and demonstrate our algorithm’s scalability with a large real-world problem in driver behaviour forecasting.

6.1 Characterizing reward recovery performance

First, we verify empirically that the reward function our algorithm learns becomes more accurate as the number of demonstration paths increases.

⁴<https://github.com/aaronsnoswell/unimodal-irl>

Table 1: Environments used for reward recovery experiment.

Environment	Dynamics	$ \mathcal{S} $	$ \mathcal{A} $	Reward Type
Taxi-v3	Stochastic starting state	500	6	$R(s, a)$
	Deterministic transitions			
FrozenLake4x4-v0	Episodic	16	4	$R(s)$
	Deterministic starting state			
	Stochastic transitions			
NChain-v0, N=10	Episodic	10	2	$R(s, a)$
	Deterministic starting state			
	Stochastic transitions			
	Continuing (non-episodic)			

As a metric for IRL algorithm performance, we choose the Inverse Learning Error (ILE), first proposed in [5]. The ILE measures the quality of a learned reward function R_L by comparing it with the ground truth reward R_{GT} — however, naïve comparison of reward values is meaningless due to the reward ambiguity problems discussed in Section 3. Instead, ILE compares *value* of the ground truth optimal policy, with the *value* of the optimal policy w.r.t. the learned reward. The ILE is given by,

$$\text{ILE} \triangleq \|\mathbf{v}(\pi_{R_{GT}}^*) - \mathbf{v}(\pi_{R_L}^*)\|_1, \quad (5)$$

where $\mathbf{v}(\pi)$ indicates the vector of state-values w.r.t. the *ground truth* reward R_{GT} for any arbitrary policy π , and $\pi_{R_{GT}}^*$ and $\pi_{R_L}^*$ denote the optimal policy w.r.t. the ground truth and learned reward functions respectively. Note that the ILE is on the range $[0, \infty)$, where lower values indicate a closer match to the ground truth reward, and the upper bound is specific to each MDP.

We evaluated the quality of our algorithm’s learned rewards on three discrete state- and action space problems from the OpenAI Gym library (shown in Table 1). For each environment, we find the optimal stationary deterministic policy using value iteration [15], then sample demonstration datasets containing an increasing number of paths. For each dataset, we learn a reward function, then compute the corresponding ILE. Each experiment is repeated 50 times to average over environment stochasticity, and we plot the ILE mean and 90% confidence intervals⁵ over the 50 repeats.

The results are shown in Fig. 2 — our algorithm always converges to a lower ILE as the number of paths increases, indicating that we are able to

⁵Unless otherwise stated, all confidence intervals we report in our experiments are symmetric.

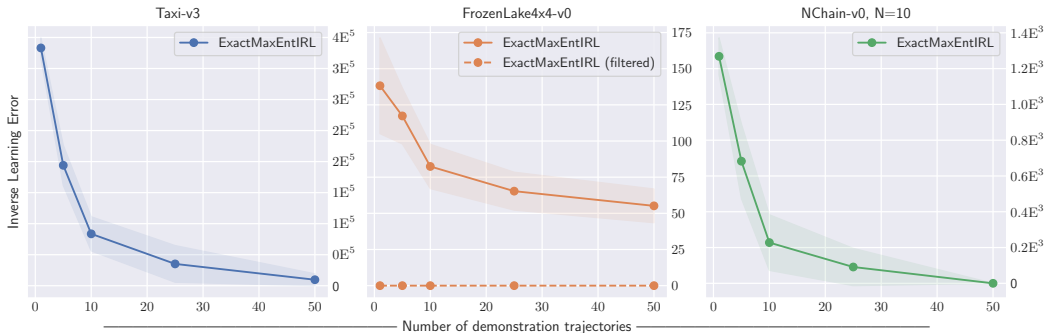


Figure 2: Our *ExactMaxEntIRL* Algorithm Performance vs. Number of Demonstration Paths, showing means and 90% confidence intervals over 50× repeats.

recover accurate reward representations, and these reward functions are more accurate with increasing numbers of demonstration paths.

Also of interest is the fact that, for the **FrozenLake4x4** environment, our algorithm converges to a non-zero ILE. We verified that this is because optimal policies in this MDP, which are used for sampling demonstrations, only solve the environment (reaching a goal state) in $\sim 82\%$ of episodes. If we artificially filter the optimal policy rollouts so that the demonstration data contain only successful episodes, our algorithm converges to 0.0 ± 0.0 ILE.

6.2 Empirical comparison with Ziebart’s algorithms

Without modification, the previous MaxEnt IRL algorithms by Ziebart *et al.* only support state-based reward features [19, 20]. The **FrozenLake4x4** environment consists of state-only rewards, which allows a fair comparison of the performance of our algorithm with these previous algorithms.

For the case of $N = 50$ demonstration paths (not filtered to remove unsuccessful demonstrations), and with 50 repeat experiments, our algorithm achieves an ILE mean and 90% confidence interval of 55.2 ± 18.3 , while Ziebart’s 2008 algorithm achieves an ILE of 634.0 ± 0.0 and the 2010 algorithm achieves an ILE of 596.7 ± 3.9 .

We also compute the log-likelihood of the demonstration data under each learned reward. Our algorithm achieves a log-likelihood mean and 90% confidence interval of -133 ± 7.78 while Ziebart’s 2008 and 2010 algorithms achieve log-likelihoods of -336 ± 31.2 and -365 ± 33.0 respectively.

For this specific environment, our algorithm out-performs Ziebart’s Maximum Entropy algorithms on the ILE metric by a factor of over $10\times$, and the log-likelihood also confirms that our rewards are a better fit to the demonstrations. These empirical data suggest that the approximate gradients from Ziebart’s algorithms can sometimes have a negative effect on reward learning, which is also reflected in the results from our driver forecasting experiment, below.

6.3 The padding trick improves computational efficiency

Without the padding trick, our algorithm has a theoretical time complexity of $\mathcal{O}(|\mathcal{S}|^2|\mathcal{A}|L^2)$, where L is the length of the longest demonstration path. With the padding trick, this dependence on L becomes linear, $\mathcal{O}(|\mathcal{S}|^2|\mathcal{A}|L)$. We verify that this difference is important in practice, not just in theory.

To illustrate this, we again use the `FrozenLake` MDP template, but randomly generate unique environments of increasing size across three orders of magnitude. For each problem size, we record the runtime required to learn a reward from a dataset of 10 paths using our algorithm in the padded, and non-padded configurations. We repeat every experiment 30 times to average over variations in processor and memory utilization. The experiments were performed on a Toshiba ThinkPad T480s laptop with an Intel i7-8650U Quad-Core CPU pinned at 2.1GHz, and with 24GB of RAM running Windows 10, 64-bit and using Python 3.6.9.

The results are shown in Fig. 3. We plot the runtime mean and 90% confidence interval vs. the problem size on a log-log scale. The empirical behaviour aligns with our theoretical complexity analysis of the algorithm: the growth rate for both versions of our algorithm is slightly higher than linear in problem size $|\mathcal{S}|^2|\mathcal{A}|$ — a line with linear gradient is shown for comparison. The results show small deviations from monotonic growth (e.g. the drop in runtime for the final point) — we hypothesise that this is due to the low-level JIT compiler we utilize to optimize the Python code.

The results also confirm that the padding trick vastly improves the computational complexity of our algorithm, and that this improvement grows with the problem size. For the small `FrozenLake4x4` MDP (problem size $\sim 10^3$, third data-point from the left in figure), we see a $\sim 10\times$ improvement in runtime, while for the larger `FrozenLake8x8` MDP (problem size $\sim 10^{4.2}$, rightmost data-point in figure), we see a $\sim 100\times$ improvement due to the padding trick. These results are very encouraging, and suggest this

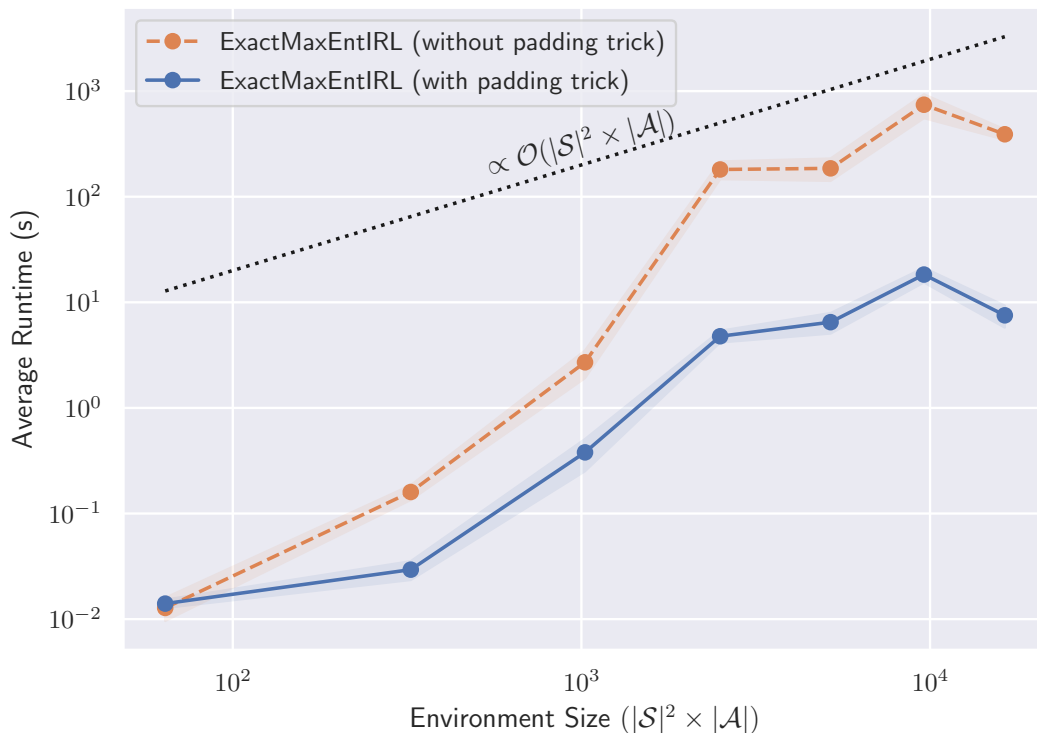


Figure 3: IRL Algorithm Runtime vs. Problem Size. Plots show mean and 90% confidence intervals over $30\times$ repeats.

algorithm is suitable for application to larger, real-world datasets, which we consider next.

6.4 Example application: forecasting driver behaviour

We demonstrate the utility of our algorithm by application to a large, real-world dataset similar to that used in the original MaxEnt IRL paper [19]. The UCI Taxi Service Prediction dataset (the ‘Porto’ dataset) contains over 1.7 million time-stamped GPS trajectories collected from the 442 taxis in the city of Porto, Portugal during 2013–14 [6].

6.4.1 Data pre-processing

We adapted the Porto dataset to make it suitable for evaluating discrete state and action IRL algorithms. Continuous GPS trajectories were fit using a par-

ticle filter to a discrete road network downloaded from OpenStreetMap.org. Trajectories were removed from the dataset if they contained missing data, were shorter than 2 minutes in duration, contained cyclic paths, ventured outside a 15km radius from the city, or if the particle filter did not converge. This resulted in an MDP with 292,604 states (road segments), 594,933 actions (unique turns at road intersections), and with a stochastic starting state and deterministic transitions. After filtering, the discretised path dataset contained 19,359 paths ranging in size from 5 to 840 states and length from 0.25 to 29km. We excluded outlier paths with more than 400 states, and segmented into a 70% training set (13551 paths) and 30% held-out test set (5808 paths).

6.4.2 Reward feature selection

To allow comparison with Ziebart’s algorithm, we selected a state-only reward feature representation. As state features we utilised the number of lanes (1, 2, or > 2), road type (‘local’, ‘major’, ‘highway’, or ‘other’), speed limit ($< 35\text{km/h}$, $35 - 55\text{km/h}$, $55 - 85\text{km/h}$, $> 85\text{km/h}$, or ‘unknown’) and toll status (‘toll’ or ‘no toll’), giving a 14-dimensional indicator vector $\mathbf{I}(s)$ which we multiplied by the distance of a road segment in meters, $\phi_s(s) \triangleq \mathbf{I}(s) \times \text{dist}(s)$.

6.4.3 Evaluation Metrics

The ILE metric used in our synthetic experiments requires that the ground truth reward function be known. In the absence of a ground truth reward function, different evaluation metric(s) must be used. We used two evaluation metrics, as follows:

- *Distance Match Percentage* $\in [0, 100]$, higher is better. Measures the percentage of distance of the predicted maximum likelihood path that matches the ground truth path. This is a domain-specific approximate measure of predictive accuracy of the policies induced by a learned reward.
- *Feature Distance* $\in [0, \infty)$, lower is better, units are km. Measures the L^2 norm between the predicted maximum likelihood path’s feature vector and that of the ground truth path. This is a domain-agnostic metric

that quantifies how well the trained model matches the demonstrated preferences in the data.

6.4.4 Results

Using optimized implementations on a 24-core cluster workstation with Intel Xeon E5-2760 v3 CPUs at 2.4Ghz and 384GB of RAM, individual models took ~ 8 hrs to train to convergence using the L-BFGS-B optimizer, while evaluating a model against the test and the training data took ~ 60 hrs.

The results are shown in Table 2. We compare the performance of our algorithm with that from [19], as well as two baseline models - an agent that always chooses the shortest (distance) path⁶, and a MaxEnt model with sampled random normal reward weights. For each model we report the distance match and feature distance metrics to three significant figures. We report the median (and 90% confidence interval of the median) as the result distributions are skewed — however the non-overlapping confidence intervals and relative performance ranking for each metric are unchanged if the mean is used instead.

The results show that our model outperforms the others on predictive accuracy (the distance match metric), as well as in preference matching (the feature distance metric). For both metrics, the algorithm from [19], and the MaxEnt model with random normal weights perform significantly worse than either our algorithm or the shortest path heuristic — by ~ 3 , and ~ 1 orders-of-magnitude for the feature distance and distance match metrics respectively.

7 Discussion

We presented new perspective and algorithms, including a new interpretation that unifies MaxEnt IRL and RE-IRL with several implications, and an efficient exact algorithm that leads to improved reward learning and is capable of scaling up to a large real-world dataset. We make an optimized implementation compatible with OpenAI Gym environments publicly available to facilitate further research and applications.

⁶This is based on the assumption that taxi drivers (or their customers) might prefer a direct route to a destination.

Table 2: Driver behaviour forecasting problem: experimental results

Algorithm	Distance Match (%) Median (90% C.I.)	Feature Distance (km) Median (90% C.I.)
ExactMaxEntIRL (Ours)	64.3 (62.4 – 66.1)	0.840 (0.797 – 0.858)
Shortest Path	50.5 (48.9 – 51.7)	0.995 (0.963 – 1.02)
Ziebart et al. 2008 [19]	31.4 (30.4 – 32.4)	178 (177 – 179)
Random Weights	27.1 (26.4 – 28.0)	220 (219 – 221)

We plan to follow up this work with some further developments. First, as mentioned in Section 2, we can develop exact algorithms to handle more complex features by adapting the sum-product algorithm. This can potentially lead to further performance improvement when complex features are indeed necessary. Second, we pointed out that our new interpretation of MaxEnt IRL suggests that we can directly adapt the model-free importance sampling learning algorithm for RE-IRL to MaxEnt IRL. While this may be biased towards short demonstrations, this allows us to deal with continuous MDPs. In addition, in principle, we can choose an alternative reference distribution to encode any other prior preference. This needs to be further explored and empirically evaluated against the exact algorithms. Lastly, the MaxEnt IRL model in fact learns a reward function for a non-stationary policy (that is, the MaxEnt trajectory distribution), however we (and others) treat the learned reward function as suitable for stationary policies, because it is computationally easier to evaluate the performance of a stationary policy. Our experiments suggest that the learned reward function are often suitable for a stationary policy. We hope to better understand when the reward function is suitable for a stationary policy, and develop an effective method of using the learned reward together with a non-stationary policy.

Acknowledgment

Aaron Snoswell is supported by through an Australian Government Research Training Program Scholarship.

8 Derivation of MaxEnt *via* Minimum KL-Divergence

Proposition 1. *The solution of Eq. 3 is given by Eq. 1.*

Proof. The Lagrangian of Eq. 3 is

$$\begin{aligned} \mathcal{L}(p(\tau_1), \dots, p(\tau_n), \lambda_1, \boldsymbol{\lambda}_2) &= \sum_{\tau \in \mathcal{T}} p(\tau) (\log p(\tau) - \log q(\tau)) \\ &+ \lambda_1 (1 - \sum_{\tau \in \mathcal{T}} p(\tau)) + \boldsymbol{\lambda}_2^\top \left(\frac{1}{|\mathcal{D}|} \sum_{\tau \in \mathcal{T}} \boldsymbol{\phi}(\tau) (1 - p(\tau)) \right) \end{aligned}$$

where λ_1 , $\boldsymbol{\lambda}_2$ are the Lagrange multipliers. We differentiate w.r.t. $p(\tau)$ and set the derivative to zero, giving,

$$\begin{aligned} \implies \log p(\tau) - \log q(\tau) + 1 &= \lambda_1 + \boldsymbol{\lambda}_2^\top \boldsymbol{\phi}(\tau) \\ p_{\boldsymbol{\theta}}(\tau) &= q(\tau) e^{\boldsymbol{\theta}^\top \boldsymbol{\phi}(\tau)} / Z_{\boldsymbol{\theta}} \end{aligned}$$

where we have re-named $\boldsymbol{\lambda}_2 \rightarrow \boldsymbol{\theta}$, and λ_1 is chosen to normalize the distribution forming the *partition function* $Z_{\boldsymbol{\theta}}$. \square

9 Analysis of Ziebart et al. MaxEnt IRL Algorithms

We briefly show that two previously published algorithms for the MaxEnt IRL problem do not always compute exact feature expectations. We encourage the reader to reference the original algorithms [19, 20] to follow the notation in the proofs.

Proposition 2. *Algorithm 1 from [19] computes incorrect feature expectations for any MDP with uniform starting state distribution and uniform dynamics, but non-uniform state reward function.*

Proof. Consider an MDP with uniform initial distribution and transition dynamics,

$$\begin{aligned} p_0(s) &\triangleq 1/|\mathcal{S}| & \forall s \in \mathcal{S} \\ T(s' | s, a) &\triangleq 1/|\mathcal{S}| & \forall s \in \mathcal{S}, a \in \mathcal{A} \end{aligned}$$

By ‘Algorithm 1’, step (4), we have $D_{s,1} = p_0(s) = 1/|\mathcal{S}| \forall s \in \mathcal{S}$. Computing the next timestep for $D_{s,t}$ using (5), we have

$$\begin{aligned}
D_{s,2} &= \sum_{a \in \mathcal{A}} \sum_{s' \in \mathcal{S}} D_{s',1} p(a | s) T(s' | s, a) \\
&= \sum_{a \in \mathcal{A}} \sum_{s' \in \mathcal{S}} \frac{1}{|\mathcal{S}|} p(a | s) \frac{1}{|\mathcal{S}|} \\
&= \left(\sum_a p(a | s) \right) \left(\sum_{s'} \frac{1}{|\mathcal{S}|^2} \right) = (1) \left(\frac{1}{|\mathcal{S}|} \right) \\
\implies D_{s,t} &= \frac{1}{|\mathcal{S}|} \quad \forall s \in \mathcal{S}, t = 1, \dots, N.
\end{aligned}$$

Thus, the computed state marginals do not depend on the reward function. This is only true for a degenerate reward $R(s) = \text{const.}$, for any non-uniform reward we will have a contradiction. \square

The same paper was updated in 2010 with minor revisions to the algorithm regarding the handling of terminal states [20]. The above proof also applies verbatim to this updated algorithm, with slightly different working

Proposition 3. *Algorithm 1 from [20] computes incorrect feature expectations for any MDP with uniform starting state distribution and uniform dynamics, but non-uniform state reward function.*

Proof. Consider the same MDP as Proposition 2, with uniform initial distribution and transition dynamics. small

$$\begin{aligned}
p_0(s) &= 1/|\mathcal{S}| & \forall s \in \mathcal{S} \\
p(s' | s, a) &= 1/|\mathcal{S}| & \forall s \in \mathcal{S}, a \in \mathcal{A}
\end{aligned}$$

By ‘Algorithm 1’, step (4), we have $D_{s,1} = p_0(s) = 1/|\mathcal{S}| \forall s \in \mathcal{S}$. Computing the next timestep for $D_{s',t}$ using (5), we have

$$\begin{aligned}
D_{s',2} &= \sum_{s \in \mathcal{S}} \sum_{a \in \mathcal{A}} D_{s,1} p(a | s) p(s' | s, a) \\
&= \sum_{s \in \mathcal{S}} \sum_{a \in \mathcal{A}} \frac{1}{|\mathcal{S}|} p(a | s) \frac{1}{|\mathcal{S}|} = \frac{1}{|\mathcal{S}|^2} \sum_{s \in \mathcal{S}} \left(\sum_a p(a | s) \right) \\
&= \frac{1}{|\mathcal{S}|^2} \sum_{s \in \mathcal{S}} (1) = \frac{1}{|\mathcal{S}|} \\
\implies D_{s',t} &= \frac{1}{|\mathcal{S}|} \quad \forall s' \in \mathcal{S}, t = 1, \dots, N
\end{aligned}$$

Once again, for any non-uniform reward there will be a contradiction. \square

References

- [1] Pieter Abbeel and Andrew Y. Ng. “Apprenticeship Learning via Inverse Reinforcement Learning”. In: *21st International Conference on Machine Learning*. Morgan Kaufmann Publishers Inc., 2004.
- [2] Navid Aghasadeghi and Timothy Bretl. “Maximum Entropy Inverse Reinforcement Learning in Continuous State Spaces with Path Integrals”. In: *IEEE/RSJ International Conference on Intelligent Robots and Systems*. IEEE, 2011, pp. 1561–1566.
- [3] Abdeslam Boularias, Jens Kober, and Jan Peters. “Relative Entropy Inverse Reinforcement Learning”. In: *Proceedings of the 14th International Conference on Artificial Intelligence and Statistics*. 2011, pp. 182–189.
- [4] Greg Brockman et al. *OpenAI Gym*. 2016. arXiv: 1606.01540.
- [5] J. D. Choi and Kee-Eung Kim. “Inverse Reinforcement Learning in Partially Observable Environments”. In: *Journal of Machine Learning Research* 12 (2011), pp. 691–730.
- [6] Dheeru Dua and Casey Graff. *UCI Machine Learning Repository*. 2017.
- [7] Chelsea Finn, Sergey Levine, and Pieter Abbeel. “Guided Cost Learning: Deep Inverse Optimal Control via Policy Optimization”. In: *33rd International Conference on Machine Learning*. 2016, pp. 49–58.
- [8] Chelsea Finn et al. *A Connection between Generative Adversarial Networks, Inverse Reinforcement Learning, and Energy-Based Models*. 2016. arXiv: 1611.03852.
- [9] Justin Fu, Katie Luo, and Sergey Levine. *Learning Robust Rewards with Adversarial Inverse Reinforcement Learning*. 2017. arXiv: 1710.11248.
- [10] Mrinal Kalakrishnan et al. “Learning Objective Functions for Manipulation”. In: *IEEE International Conference on Robotics and Automation*. IEEE, 2013, pp. 1331–1336.

- [11] Frank R Kschischang, Brendan J Frey, and H-A Loeliger. “Factor graphs and the sum-product algorithm”. In: *IEEE Transactions on information theory* 47.2 (2001), pp. 498–519.
- [12] John Lafferty, Andrew McCallum, and Fernando CN Pereira. “Conditional Random Fields: Probabilistic Models for Segmenting and Labeling Sequence Data”. In: (2001).
- [13] Siu Kwan Lam, Antoine Pitrou, and Stanley Seibert. “Numba: A LLVM-Based Python JIT Compiler”. In: *Proceedings of the 2nd Workshop on the LLVM Compiler Infrastructure in HPC*. Association for Computing Machinery, 2015.
- [14] Andrew Y. Ng, Daishi Harada, and Stuart Russell. “Policy Invariance under Reward Transformations: Theory and Application to Reward Shaping”. In: *16th International Conference on Machine Learning*. Vol. 1. Morgan Kaufmann Publishers Inc., 1999, pp. 278–287.
- [15] Martin L. Puterman and Moon Chirl Shin. “Modified Policy Iteration Algorithms for Discounted Markov Decision Problems”. In: *Management Science* 24.11 (1978), pp. 1127–1137.
- [16] Markus Wulfmeier et al. “Large-Scale Cost Function Learning for Path Planning Using Deep Inverse Reinforcement Learning”. In: 36.10 (2017), pp. 1073–1087.
- [17] Brian D. Ziebart. “Modeling Purposeful Adaptive Behavior with the Principle of Maximum Causal Entropy”. PhD thesis. Carnegie Mellon University, 2010.
- [18] Brian D. Ziebart, J. Andrew Bagnell, and Anind K. Dey. “Modeling Interaction via the Principle of Maximum Causal Entropy”. In: *27th International Conference on Machine Learning*. Morgan Kaufmann Publishers Inc., 2010.
- [19] Brian D. Ziebart et al. “Maximum Entropy Inverse Reinforcement Learning”. In: *22nd AAAI Conference on Artificial Intelligence*. Vol. 8. AAAI Press, Palo Alto, California USA, 2008, pp. 1433–1438. URL: <https://www.aaai.org/Papers/AAAI/2008/AAAI08-227.pdf>.

- [20] Brian D. Ziebart et al. “Maximum Entropy Inverse Reinforcement Learning (manuscript updated)”. In: *22nd AAAI Conference on Artificial Intelligence*. Vol. 8. AAAI Press, Palo Alto, California USA, 2010, pp. 1433–1438. URL: <http://www-cgi.cs.cmu.edu/afs/cs.cmu.edu/Web/People/bziebart/publications/maxentirl-bziebart.pdf>.